Supplementary Information

Reduction of Bulk and Interface Defects via Photo-annealing Treatment for High-efficiency Antimony Selenide Solar Cells

Xiaoyang Liang*, Xinhua Wang, Qiwei Chang, Bingxin Yang, Wei Dang, Zheng Zhang, Yingnan Guo, Lin Yang, Zhiqiang Li*

Hebei Province Optoelectronic Information Materials Laboratory, College of Physics Science and Technology, Institute of Life Science and Green Development, Hebei University, Baoding 071002, China

E-mail: liangxiaoyang@hbu.edu.cn, lizhiqiang@hbu.edu.cn.

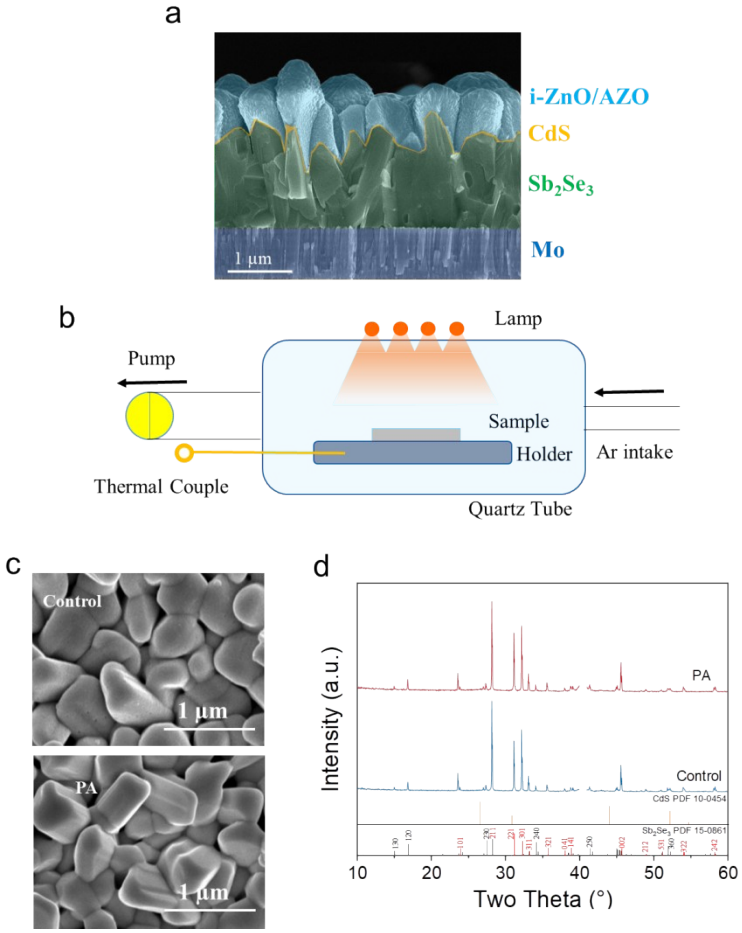

Figure S1. (a) The photograph and device structure of Sb_2Se_3 device. (b) Schematic diagram of the photon-annealing treatment system. (c) The device structure and cross-sectional SEM image of PA device

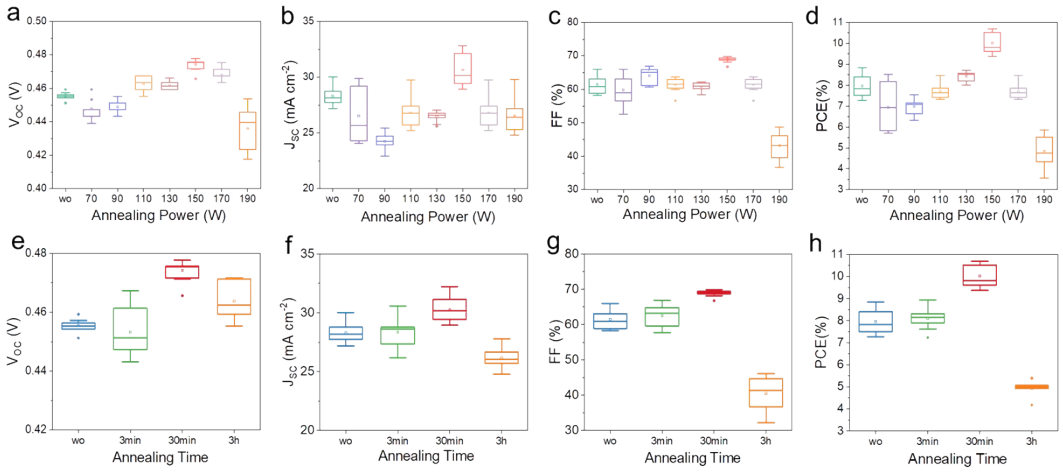

Figure S2. The device performance of the PA devices with (a-d) various heat powers and (e-h) various treatment durations. The optimal device performance is obtained with a heat power of 150 W and a duration of 30 min.

Appendix: Summary of the Report
Report No.: GXgf2023-05788
Client: Hebei University
Sample: Sb_2Se_3 solar cells
Type/Model: Sb_2Se_3 solar cells
DUT S/N: 1205-04-M3
Manufacturer: Hebei University
Sample temperature: (25±1)℃
Date of Test: 12/27/2023
Environmental conditions: (22±1) ℃, RH (18±2) %
Mask: An aperture area of 26.023 mm^2 (M1#, Certificate No.: CDjc2018-3929)

The test has been conducted by the PV Metrology Lab of NIM (National Institute of Metrology, China). Measurement of irradiance intensity and all other measurements are traceable to the International System of Units (SI). Data in this report apply only at the time of the test for the sample. For more details, please refer to the text of the report.

	Area (mm^2)	I_{sc}(mA)	V_{oc}(V)	P_{max}(mW)
Reverse Scan	26.023	7.983	0.477	2.649
Forward Scan	26.023	8.003	0.475	2.626
	I_{max}(mA)	V_{max}(V)	FF (%)	η (%)
Reverse Scan	6.793	0.390	69.63	10.18
Forward Scan	6.910	0.380	69.13	10.09

I-V Characterization Methods:
JJF 1622-2017: Calibration Specification of Solar Cells：Photoelectric Properties
Reference Solar Cell:
Type: Mono-Si
Solar Simulator:
Classification: A+AA+ (Double-light source: Xeon and Halogen);
Total irradiance: 1000 W/m^2 based on I_{sc} of the above Reference Solar Cell.

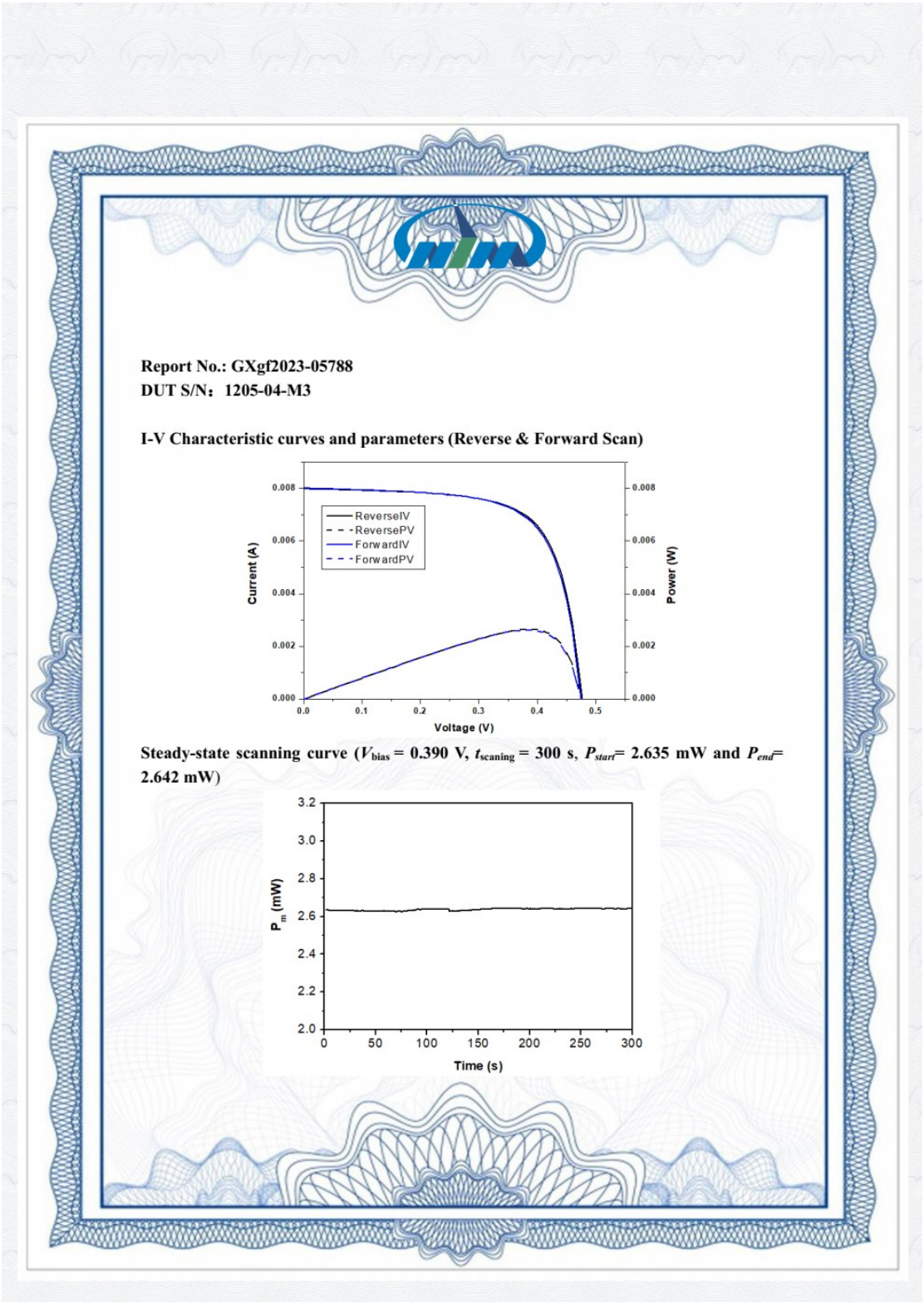

Report No.: GXgf2023-05788
DUT S/N：1205-04-M3

I-V Characteristic curves and parameters (Reverse & Forward Scan)

Steady-state scanning curve (V_{bias} = 0.390 V, $t_{scaning}$ = 300 s, P_{start}= 2.635 mW and P_{end}= 2.642 mW)

Figure S3. Certificate of the PA device by National institute of Metrology, China.

Table S1 Summary of the state-of-the-art Sb_2Se_3 solar cells with different fabrication methods

Methods	Device configuration	PCE (%)	V_{OC} (V)	J_{SC} (mA cm^{-2})	FF (%)	Year	Ref.
Hydrothermal	FTO/CdS/Sb_2Se_3/Spiro-OMeTAD/Au	7.9	0.449	28.3	62.1	2021	1
Chemical bath deposition (CBD)	FTO/CdS/Sb_2Se_3/Spiro-OMeTAD/Au	10.57	0.467	33.52	67.64	2022	2
	(FTO)/$Cd_xZn_{1-x}S$/Sb_2Se_3/Spiro-OMeTAD/Au	8.76	0.458	28.13	67.85	2024	3
Spin-coating	FTO/CdS/Sb_2Se_3/Spiro-OMeTAD/Au	5.4	0.360	29.0	51.5	2020	4
Molecular beam epitaxy (MBE)	FTO/CdS/Sb_2Se_3/Spiro-OMeTAD/Au	8.42	0.427	32.04	61.50	2024	5
Thermal evaporation (TE)	FTO/CdS/Sb_2Se_3/Spiro-OMeTAD/Au	8.90	0.448	30.36	65.44	2024	6
Pulsed laser deposition (PLD)	FTO/SnO_2/CdS/Sb_2Se_3/Au	4.77	0.334	31.68	45.04	2020	7
Vapor transport deposition (VTD)	Mo/Sb_2Se_3/CdS/ITO/Ag	8.03	0.492	26.21	62.30	2024	9
	ITO/CdS/Sb_2Se_3/Au	7.6	0.42	29.9	60.4	2018	8
	Mo/Sb_2Se_3/CdS/ITO/Ag	7.40	0.513	24.56	58.74	2022	10
Co-evaporation (CE)	Mo/Sb_2Se_3/CdS/ZnO/AZO/Au	4.51	0.376	25.39	47.24	2019	11
Magnetron sputtering deposition (MSD)	Mo/Sb_2Se_3/CdS/ITO/Ag	8.64	0.52	27.8	59.8	2022	12
	Mo/MoO_2/Sb_2Se_3/CdS:Al/ITO/Ag	8.41	0.487	28.26	60.87	2023	13
	Mo/MoO_3/Sb_2Se_3/CdS/ITO/Ag	8.23	0.479	26.46	46.93	2024	14
Rapid thermal evaporation (RTE)	Mo/Sb_2Se_3/CdS/ZnO/ITO/Ag	8.12	0.468	27.7	62.6	2023	15
	FTO/CdS/Sb_2Se_3/Au	7.57	0.41	30.5	60.51	2023	16
	Mo/Sb_2Se_3/CdS/ZnO/ITO/Ag	6.35	0.42	24.39	62.00	2023	17
Close-spaced sublimation (CSS)	Mo/ Sb_2Se_3/TiO_2/CdS/ZnO/AZO	9.2	0.40	32.58	70.3	2019	18
	FTO/TiO_2/Sb_2Se_3/P3HT/Au	8.12	0.432	32.5	57.9	2024	19
	Mo/Sb_2Se_3/CdS/ZnO/AZO/Ag	8.5	0.505	27.74	60.7	2022	20
Injection vapor deposition (IVD)	Mo/Sb_2Se_3/CdS/ZnO/AZO/Au	10.12	0.488	30.86	67.19	2022	21
	Mo/Sb_2Se_3/CdS/ZnO/AZO/Au	10.41	0.445	31.50	67.91	2024	22
	Mo/Sb_2Se_3/CdS/ZnO/AZO/Au	10.58	0.478	31.67	69.90	2024	This work

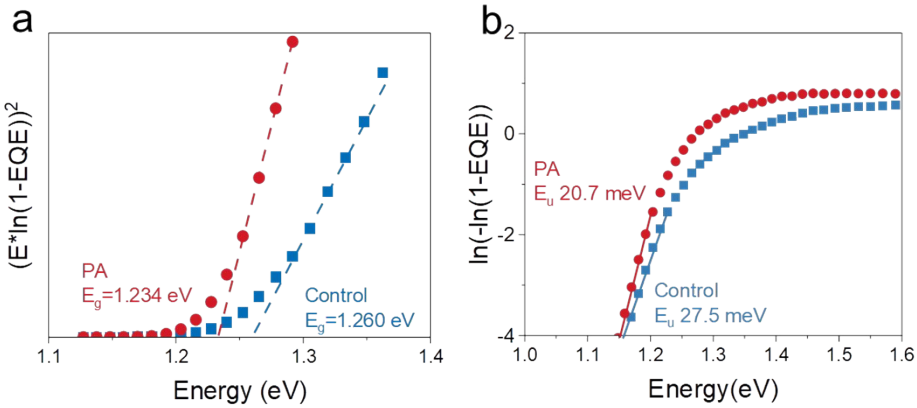

Figure S4 (a) bandgap and (b) Urbach energy derived from the EQE data of the control and PA devices.

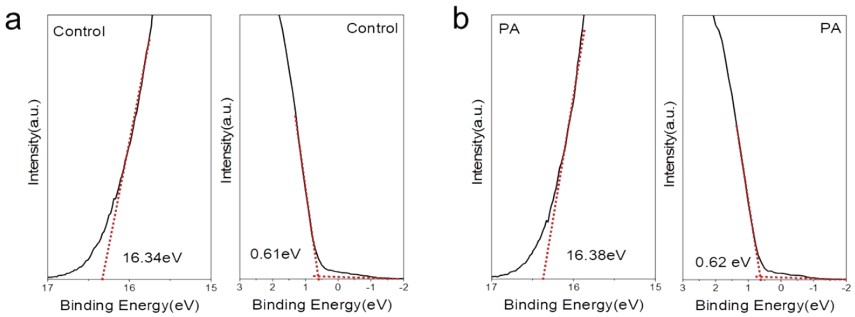

Figure S5. The UPS spectra of Sb_2Se_3 of the control (a) and PA samples (b).

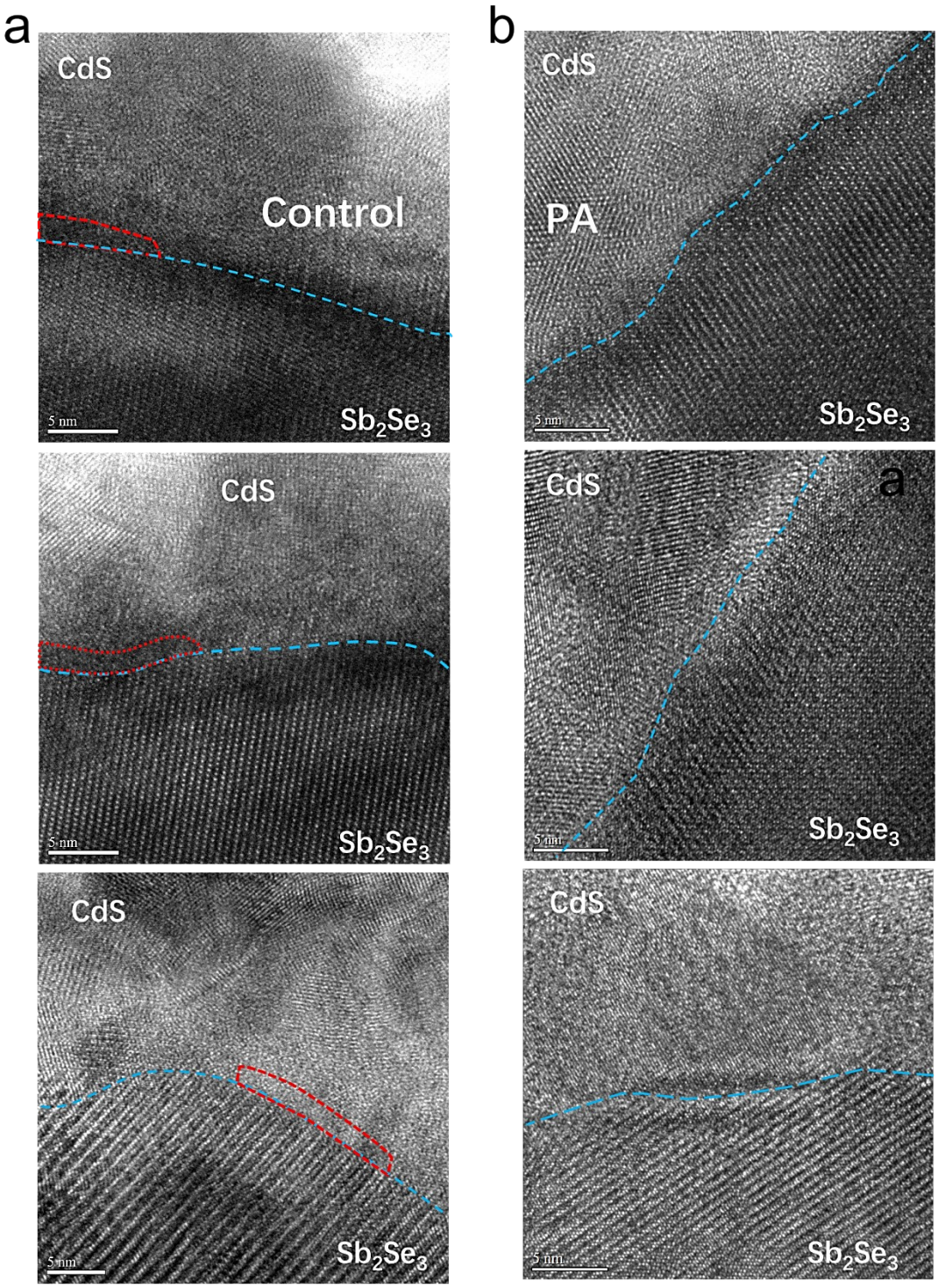

Figure S6 HRTEM image of different regions at the Sb_2Se_3/CdS heterointerface.

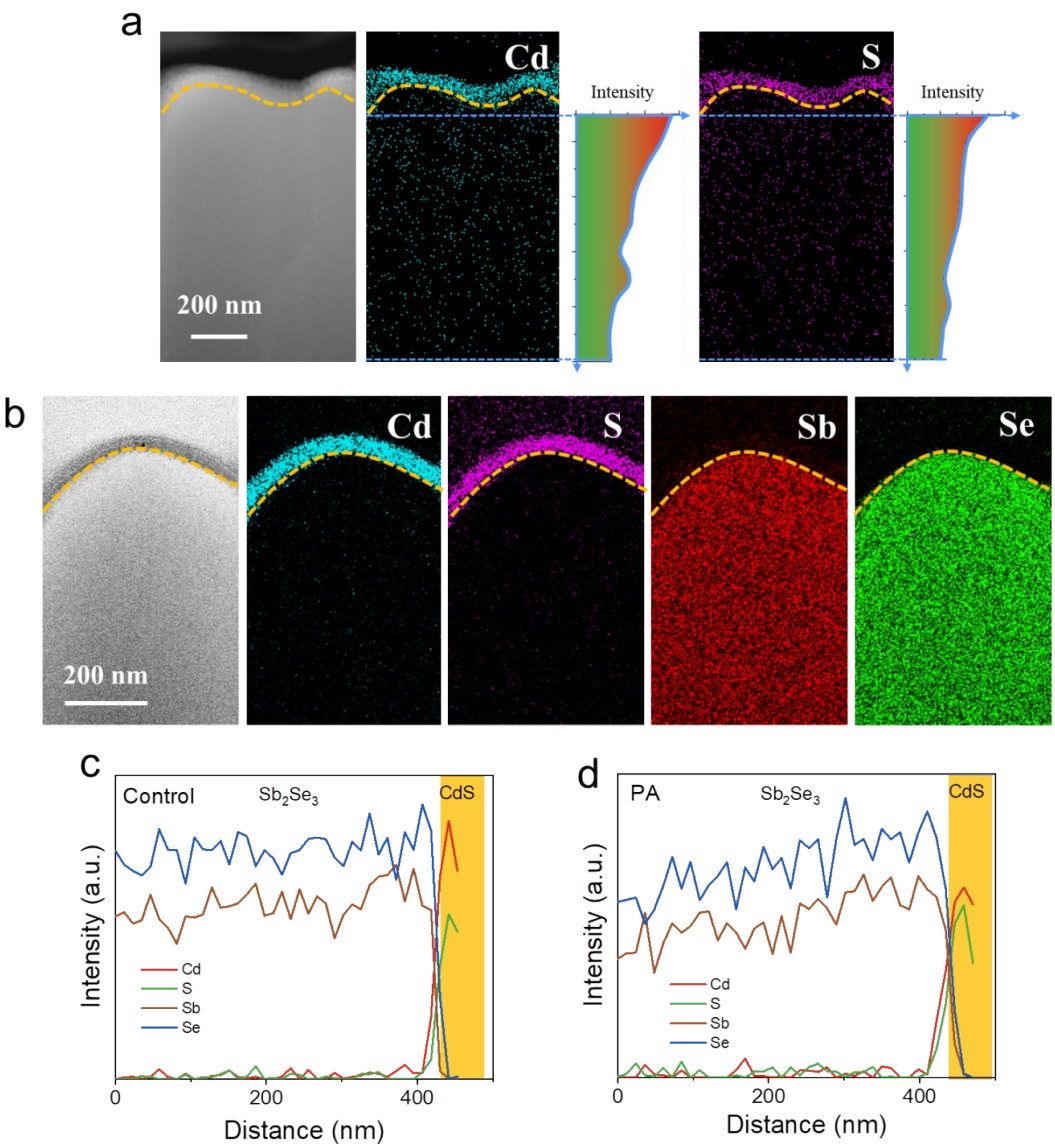

Figure S7 Energy-dispersive X-ray spectroscopy elemental mapping of PA sample (a) and Control sample (b); (c, d) the EDX line scan profiles of Control sample and PA sample

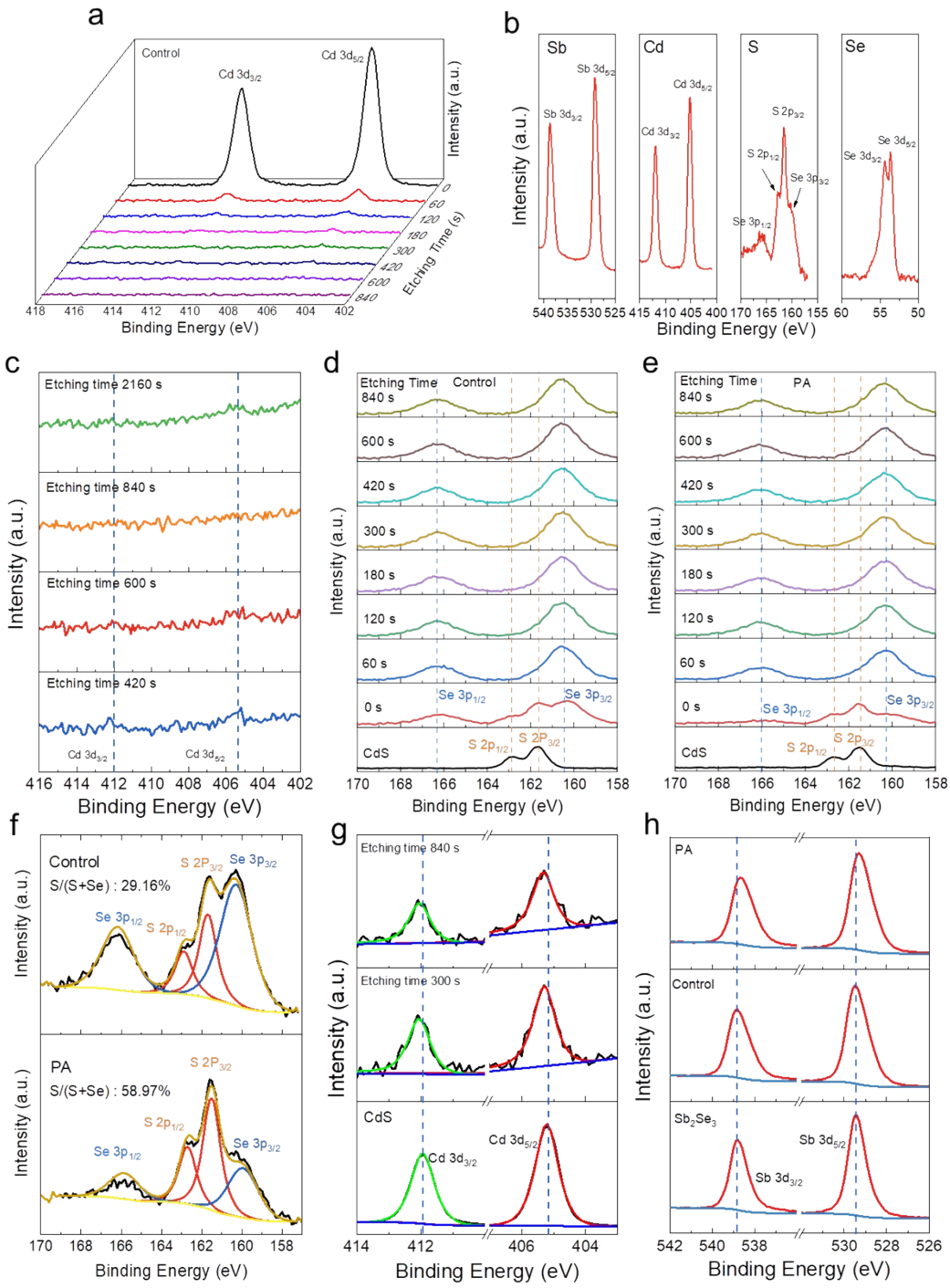

Figure S8. XPS spectra of CdS layers and Sb_2Se_3 of the control sample with different etching time. (a) (c) In-depth Cd 3d XPS spectra with different etching time of the Control sample. (b) The Sb 3d, Cd 3d, S 2p and Se 3d spectra of PA sample. (d) (e) The relative S component on the surfaces of Control sample and PA sample. (f) The relative S component on the surfaces of Control sample and PA sample. (g) The

Cd 3d XPS spectra of CdS and PA sample. (h) The Sb 3d spectra of the Sb_2Se_3 (unprepared with CdS buffer), the Control sample and the PA sample

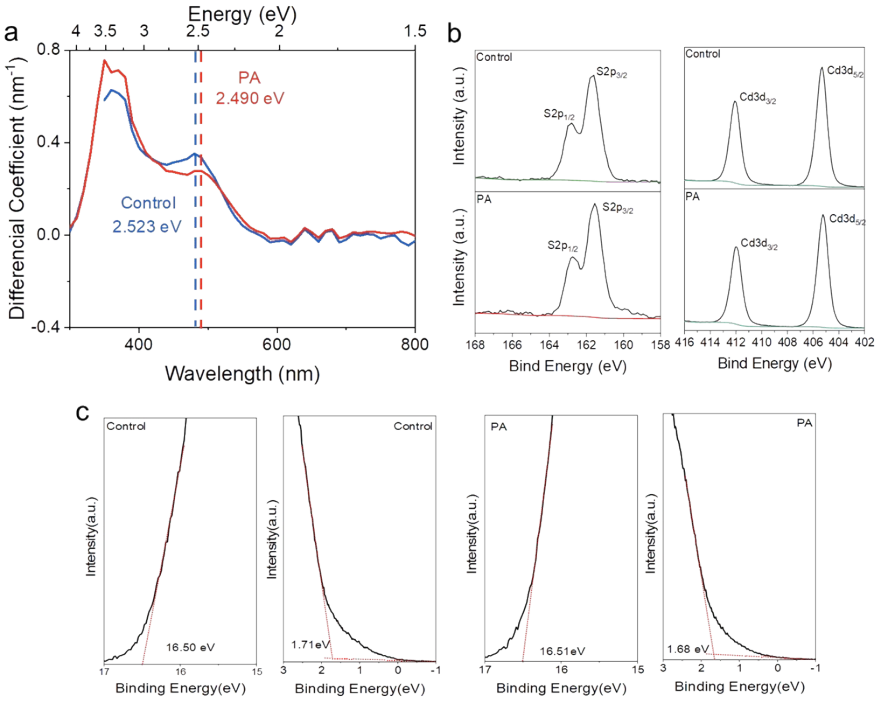

Figure S9 (a) The differential EQE spectra for the control and PA devices. (b) The S 2p and Se 3d spectra for the control and PA devices. (c) The UPS spectra of Sb_2Se_3 of CdS buffer layer for the control and PA samples.

We calculated the bandgap of CdS from the differential EQE spectra as shown In Figure S8a. Following PA treatment, a minute reduction in the optical bandgap of the CdS films was achieved, narrowing it from 2.523 eV to 2.490 eV. Moreover, Figures S8d exhibits the XPS spectra for the Cd and S elements of CdS films. No discernible differences in the elemental chemical states were found between the two thin films, indicating that no significant phase transition occurred in the CdS during PA treatment. To establish the band diagram of the CdS buffer layers, UPS measurements were conducted. For the control sample, the Fermi energy, valence band maximum (VBM), and conduction band maximum (CBM) of CdS were calculated to be -4.72 eV, -6.43 eV, and -3.91 eV, respectively. For the PA-treated sample, these values were -4.71 eV, -6.39 eV, and -3.90 eV, respectively. Notably, the positions of the Fermi level and valence band in CdS remained relatively unchanged during the PA treatment. This phenomenon may be linked to the reduction of wide bandgap hydroxide species, such as OH^- or O^{2-}. The results show that the PA treatment has little to no effect on CdS buffer layer.

References

1. D. Liu, R. Tang, Y. Ma, C. Jiang, W. Lian, G. Li, W. Han, C. Zhu and T. Chen, *ACS applied materials & interfaces*, 2021, **13**, 18856-18864.
2. Yuqi Zhao, Shaoying Wang, Chuang Li, Bo Che, Xueling Chen, Hongyi Chen, Rongfeng Tang, Xiaomin Wang, Guilin Chen, Ti Wang, Junbo Gong, Tao Chen, Xudong Xiao and a. J. Li, *Energy and Environmental Science*, 2022.
3. Y. Yang, T. Zhang, H. Zhu, K. Geng, S. Huang, B. Shen, B. Dong, S. Zhang, D. Gu, S. Jiang, Y. Yan, H. Guo, J. Qiu, L. Li, N. Yuan and J. Ding, *Small*, 2024, DOI: 10.1002/smll.202403292, e2403292.
4. Y. Ma, B. Tang, W. Lian, C. Wu, X. Wang, H. Ju, C. Zhu, F. Fan and T. Chen, *Journal of Materials Chemistry A*, 2020, **8**, 6510-6516.
5. K. Li, J. Yang, Z. Cai, Y. Gu, A. Liu, C. Zhu, R. Tang and T. Chen, *Small methods*, 2024, DOI: 10.1002/smtd.202400227, e2400227.
6. Z. Cai, B. Che, Y. Gu, P. Xiao, L. Wu, W. Liang, C. Zhu and T. Chen, *Advanced Materials*, 2024, DOI: 10.1002/adma.202404826, e2404826.
7. K. Yang, B. Li and G. Zeng, *Journal of Alloys and Compounds*, 2020, **821**, 153505.
8. M. Chen, M. Ishaq, D. Ren, H. Ma, Z. Su, P. Fan, D. Le Coq, X. Zhang, G. Liang and S. Chen, *Journal of Energy Chemistry*, 2024, **90**, 165-175.
9. X. Wen, C. Chen, S. Lu, K. Li, R. Kondrotas, Y. Zhao, W. Chen, L. Gao, C. Wang, J. Zhang, G. Niu and J. Tang, *Nature communications*, 2018, **9**, 2179.
10. G. Liang, M. Chen, M. Ishaq, X. Li, R. Tang, Z. Zheng, Z. Su, P. Fan, X. Zhang and S. Chen, *Advanced science*, 2022, **9**, e2105142.
11. Z. Li, H. Zhu, Y. Guo, X. Niu, X. Chen, C. Zhang, W. Zhang, X. Liang, D. Zhou, J. Chen and Y. Mai, *Applied Physics Express*, 2016, **9**, 052302.
12. R. Tang, S. Chen, Z. H. Zheng, Z. H. Su, J. T. Luo, P. Fan, X. H. Zhang, J. Tang and G. X. Liang, *Advanced Materials*, 2022, DOI: 10.1002/adma.202109078, e2109078.
13. Y. Luo, G. Chen, S. Chen, N. Ahmad, M. Azam, Z. Zheng, Z. Su, M. Cathelinaud, H. Ma, Z. Chen, P. Fan, X. Zhang and G. Liang, *Advanced Functional Materials*, 2023, **33**.
14. J. Yang, M. Chen, G. Chen, Y. Hou, Z. Su, S. Chen, J. Zhao and G. Liang, *Advanced science*, 2024, **11**.
15. X. Liu, Y. Liu, S. Zhang, X. Sun, Y. Zhuang, J. Liu, G. Wang, K. Cheng and Z. Du, *Small methods*, 2024, **8**, e2300728.
16. H. Guo, S. Huang, H. Zhu, T. Zhang, K. Geng, S. Jiang, D. Gu, J. Su, X. Lu, H. Zhang, S. Zhang, J. Qiu, N. Yuan and J. Ding, *Advanced science*, 2023, **10**, e2304246.
17. Y. Liu, X. Liu, Y. Zhuang, E. Li, S. Zhang, J. Liu, K. Cheng and Z. Du, *Journal of Alloys and Compounds*, 2023, **949**, 169729.
18. Z. Li, X. Liang, G. Li, H. Liu, H. Zhang, J. Guo, J. Chen, K. Shen, X. San, W. Yu, R. E. I. Schropp and Y. Mai, *Nature communications*, 2019, **10**, 125.
19. C. H. Don, T. P. Shalvey, D. A. Sindi, B. Lewis, J. E. N. Swallow, L. Bowen, D. F. Fernandes, T. Kubart, D. Biswas, P. K. Thakur, T. L. Lee and J. D. Major, *Advanced Energy Materials*, 2024, DOI: 10.1002/aenm.202401077.
20. S. Rijal, D. B. Li, R. A. Awni, C. Xiao, S. S. Bista, M. K. Jamarkattel, M. J. Heben, C. S. Jiang, M. Al-Jassim, Z. Song and Y. Yan, *Advanced Functional Materials*, 2021, **32**, 2110032.
21. Z. Duan, X. Liang, Y. Feng, H. Ma, B. Liang, Y. Wang, S. Luo, S. Wang, R. E. I. Schropp, Y. Mai

and Z. Li, *Advanced Materials*, 2022, **34**, e2202969.

22. A. Mo, Y. Feng, B. Yang, W. Dang, X. Liang, W. Cao, Y. Guo, T. Chen and Z. Li, *Advanced Functional Materials*, 2024, DOI: 10.1002/adfm.202316292.